Fortschritte der Physik, 27 June 2012

Status of three–neutrino oscillation parameters

Mariam Tórtola[1,*]

[1] AHEP Group, Instituto de Física Corpuscular – C.S.I.C./Universitat de València
Edificio de Institutos de Paterna, Apartado 22085, E–46071 València, Spain

Received XXXX, revised XXXX, accepted XXXX
Published online XXXX

Key words Neutrino mass and mixing, neutrino oscillations, solar and atmospheric neutrinos, reactor and accelerator neutrinos.

Here we review the current status of global fits to neutrino oscillation data within the three-flavour framework. In our analysis we include the most recent data from solar and atmospheric neutrino experiments as well as the latest results from the long-baseline accelerator neutrino experiments and the recent measurements of reactor neutrino disappearance reported by Double Chooz, Daya Bay and RENO. We present updated determinations for the two neutrino mass splittings and the three mixing angles responsible for neutrino oscillations that, for the first time, have all been measured with 1σ accuracies ranging from 3 to 15%. A weak sensitivity for the CP violating phase δ is also reported from the global analysis.

1 Introduction

Prompted by the observed anomalies in the solar and atmospheric neutrino fluxes, a rich variety of neutrino oscillation experiments has been proposed along the last decade. Today a large amount of experimental data provides convincing evidence for neutrino oscillations in solar and atmospheric neutrino experiments as well as in reactor and long-baseline accelerator experiments. Thanks to the good quality and the complementarity of the different experimental data sets we have now a pretty accurate determination of the parameters governing three-flavour neutrino oscillations.

The paper is organized as follows. In Sec. 2 we briefly describe the solar neutrino experiments included in the analysis and the KamLAND reactor neutrino experiment, and discuss the determination of the leading oscillation parameters in the solar sector Δm^2_{21} and θ_{12} from the combination of KamLAND and solar neutrino experiments. In Sec. 3 we discuss the determination of the leading oscillation parameters in the atmospheric neutrino sector Δm^2_{31} and θ_{23} by the combination of the full Super-Kamiokande atmospheric neutrino data sample with the long-baseline accelerator data from the K2K and MINOS experiments, that provide an independent confirmation of the atmospheric neutrino oscillations. After describing the dominant oscillations in the solar and atmospheric neutrino sectors, we devote Sec. 4 to the determination of the reactor mixing angle θ_{13}. We discuss the constraints on θ_{13} coming from the interplay of the solar + KamLAND and atmospheric + accelerator data samples, from the electron neutrino appearance searches at long-baseline experiments and finally from the recent measurements reported by the new generation of reactor experiments The results from the three-neutrino global analysis of current neutrino data (obtained in Refs. [1–3]) are summarized in Sec. 5. There we present the best fit values and allowed ranges for all the neutrino oscillation parameters. Finally we conclude in Sec. 6 with a summary of the presented results and a short discussion about the future prospects in neutrino oscillation physics.

* E-mail: mariam@ific.uv.es,

2 The solar neutrino sector

2.1 Solar neutrino data

We include in our analysis the latest solar neutrino data from the radiochemical experiments Homestake [4], Gallex + GNO [5] and SAGE [6]. The most relevant information for the determination of the oscillation neutrino parameters, however, comes from the real-time experiments Super-Kamiokande (SK) and Sudbury Neutrino Observatory (SNO).

The Super-Kamiokande experiment, located at the Kamioka mine in Japan, is a Cherenkov detector that uses 50 kton of ultra pure water (with a fiducial volume of 22.5 kton for solar neutrino measurements) as target for the interactions of the solar neutrinos, detected through elastic neutrino-electron scattering: $\nu_x + e^- \to \nu_x + e^-$. The scattered electrons produce Cherenkov light which is detected by the photomultipliers that cover the internal part of the detector. The experiment is sensitive to all active neutrino flavors through the neutral-current interaction, although the main contribution comes from ν_e, due to the larger value of the charged-current cross section. The existence of a directional correlation between the incident neutrino and the recoil electron in the elastic scattering allows the reconstruction of the incoming neutrino energy. Here we consider the solar neutrino data from the three phases of the Super-Kamiokande experiment [7–9]. The three data samples (SK-I, SK-II and SK-III) have been collected with different exposure times and neutrino energy thresholds and are presented in the form of day/night or zenith-angle spectrum, providing information about the incident neutrino energy and the arrival neutrino direction. So far the Super-Kamiokande solar neutrino data has not reported the presence of spectral distortions or day/night asymmetries in the solar neutrino flux.

The Sudbury Neutrino Observatory (SNO) is a water Cherenkov detector filled with 1000 tonnes of pure heavy water (D_2O) contained in a 12 m diameter acrylic sphere. It is located 2 km underground in the Creighton mine near Sudbury, Canada. The heavy water in SNO provides deuterons as a target for charged-current (CC) and neutral-current (NC) weak interactions, as well as electrons for elastic scattering (ES) processes with solar neutrinos:

$$\begin{array}{ll} \nu_e + d \to p + p + e^- & (\mathrm{CC}) \\ \nu_x + d \to n + p + \nu_x & (\mathrm{NC}) \\ \nu_x + e^- \to \nu_x + e^- & (\mathrm{ES}) \end{array} \qquad (1)$$

By measuring the rate of CC and NC events, SNO is able to determine the electron neutrino ν_e flux and the total active ν_x flux of ^{8}B neutrinos from the Sun. In the CC and ES reactions, the recoiling electron emits Cherenkov light detected by 9456 photomultiplier tubes (PMTs) mounted on a geodesic support structure surrounding the heavy water vessel. The detector is immersed in ultra–pure light water to provide shielding against radioactive backgrounds from the geodesic structure and the cavity rock. For the NC reaction, the signal is the appearance of a free neutron in the detector. The liberated neutron is then thermalized in the heavy water as it scatters around and it is finally captured by another nucleus. The way in which this neutron is detected is what characterizes the three running phases of the SNO experiment. In phase I neutrons were captured on deuterons, in phase II 2 tonnes of NaCl were added to enhance the neutron capture efficiency on chlorine, while in the last phase neutrons were mainly detected by an array of ^{3}He proportional counters. Here we use the neutrino oscillation data from the three phases of SNO [10, 11].

The direct measurement of the ^{7}Be solar neutrino signal rate performed by the Borexino collaboration [12] is also considered in our analysis. An interaction rate of the 0.862 MeV ^{7}Be neutrinos of 49$\pm$3(stat)$\pm$4(syst) counts/(day·100 ton) has been reported. This measurement constitutes the first direct determination of the survival probability for solar ν_e in the transition region between matter-enhanced and vacuum-driven oscillations. The survival probability of 0.862 MeV ^{7}Be neutrinos is determined to be $P_{ee}^{^7\mathrm{Be,obs}} = 0.56 \pm 0.1$. Given the present uncertainties, for the moment Borexino plays no significant role in the determination of neutrino oscillation parameters, but the observed neutrino survival probability is in perfect agreement with all the other solar data.

For our simulation of the production and propagation of neutrinos in the Sun we consider the most recent update of the standard solar model [13], fixing our calculations to the low metalicity model labelled as AGSS09. The impact of the choice of a particular solar model over the neutrino oscillation analysis has been discussed in the arXiv updated version of Ref. [14]. The analysis methods used here are similar to the ones described in [15] and references therein, including the use of the so-called pull approach for the χ^2 calculation, as described in Ref. [16]. In this method all systematic uncertainties are included by introducing new parameters in the fit and adding a penalty function to the χ^2.

2.2 The KamLAND reactor experiment

KamLAND is a reactor neutrino experiment with its detector located at the Kamiokande site. Most of the $\bar{\nu}_e$ flux incident at KamLAND comes from nuclear plants at distances of $80 - 350$ km from the detector, making the average baseline of about 180 kilometers, long enough to probe the solar neutrino oscillations with $\Delta m^2_{21} \sim 10^{-5}\text{eV}^2$. The KamLAND collaboration has for the first time measured the disappearance of neutrinos traveling to a detector from a power reactor [17]. They have observed a strong evidence for the disappearance of neutrinos during their flight over such distances, giving the first terrestrial confirmation of the solar neutrino anomaly and also establishing the oscillation hypothesis with man-produced neutrinos. In KamLAND the reactor antineutrinos are observed by the inverse beta decay process $\bar{\nu}_e + p \to e^+ + n$, where the delayed coincidence of the prompt energy from the positron and a characteristic gamma from the neutron capture allows an efficient reduction of backgrounds. The neutrino energy is related to the prompt energy by $E_\nu = E_{\rm pr} + \Delta - m_e$, where Δ is the neutron-proton mass difference and m_e is the positron mass.

In our global analysis of neutrino oscillation data we consider the most recent results published by the KamLAND reactor experiment with a total livetime of 2135 days, including the data collected during the radiopurity upgrade in the detector [18]. After all selection cuts a total of 2106 reactor antineutrino events have been observed in the detector while 2879$\pm$118 reactor antineutrino events together with 325.9$\pm$26.1 background events were expected in the absence of neutrino oscillations. For our simulation we use the recent re-evaluation of the reactor anti-neutrino fluxes given in [19] and include various systematic errors associated to the neutrino fluxes, reactor fuel composition and individual reactor powers. Matter effects are also considered in our simulation, as well as a careful treatment of backgrounds and information on the average contribution to the total reactor neutrino signal as a function of the distance to the detector. To avoid large uncertainties associated with the geo-neutrino flux present at lower energies, an energy cut at 2.6 MeV prompt energy is applied for the oscillation analysis.

The KamLAND allowed regions for $\sin^2\theta_{12}$ and Δm^2_{21} are shown in Fig. 1 (blue lines) in comparison with the regions from solar data (black lines). As can be seen from the figure, the oscillation parameters derived from the KamLAND-only antineutrino data are in good agreement with those of the solar-only neutrino data.

2.3 Combined solar + KamLAND analysis

Fig. 1 illustrates how the determination of the leading solar oscillation parameters θ_{12} and Δm^2_{21} emerges from the complementarity of solar and KamLAND neutrino data. From the global three-flavour analysis we find the following best fit points (with 1σ errors):

$$\sin^2\theta_{12} = 0.320^{+0.015}_{-0.017}\,, \qquad \Delta m^2_{21} = 7.62 \pm 0.19 \times 10^{-5}\,\text{eV}^2\,. \tag{2}$$

The spectral information from KamLAND data leads to an accurate determination of Δm^2_{21} with a 2.5% 1σ uncertainty. The main limitation for the Δm^2_{21} measurement comes from the uncertainty on the energy scale in KamLAND that produces a 1.8% error on Δm^2_{21} [18] . KamLAND data start also to contribute to the lower bound on $\sin^2\theta_{12}$, whereas the upper bound is dominated by solar data, most importantly by the CC/NC solar neutrino rate measured by SNO.

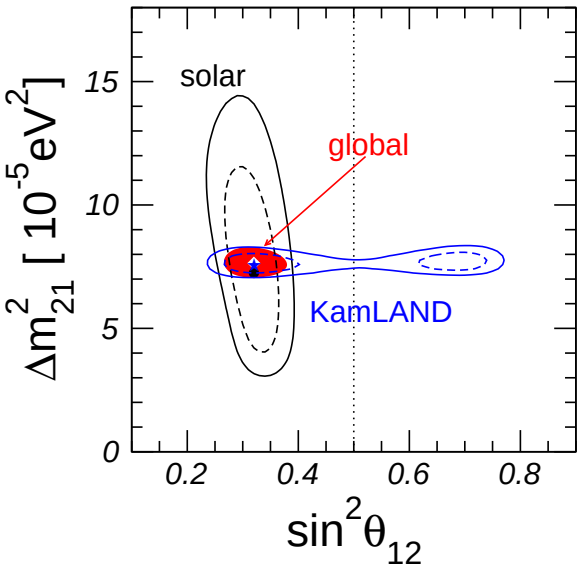

Fig. 1 Determination of the solar oscillation parameters from the interplay of data from all solar neutrino experiments and KamLAND. We show the allowed regions at 90% and 3σ CL (2 dof) for solar and KamLAND, as well as the 3σ region for the combined analysis. The dot, star and diamond indicate the best fit points of solar data, KamLAND and global data, respectively. We minimise with respect to Δm^2_{31}, θ_{23} and θ_{13}, including always atmospheric, long-baseline and reactor data.

3 The atmospheric neutrino sector

3.1 Atmospheric neutrino data

After several years observing a deficit in the detected number of atmospheric neutrinos with respect to the predictions, in 1998 the Super-Kamiokande collaboration obtained evidence for neutrino oscillations [20] from the observation of the zenith angle dependence of their μ-like atmospheric neutrino data. Subsequently, Super-Kamiokande data showed a dip in the L/E distribution of the atmospheric ν_μ survival probability [21], providing a clear signature for neutrino oscillations.

In this analysis we include the full sample of atmospheric neutrino data from all three phases of the Super-Kamiokande experiment [22], using directly the χ^2 map provided by the Super-Kamiokande collaboration. All types of atmospheric neutrino events defined by Super-Kamiokande (fully contained, partially contained and upward-going muons, plus further divisions into additional sub-samples) collected almost continuously from 1996 until June 2007 have been considered for the analysis. Improved reconstruction algorithms and Monte-Carlo simulations have also been incorporated. The atmospheric neutrino oscillation analysis has been performed within the one mass scale approximation, neglecting the effect of the solar mass splitting. The allowed regions for the oscillation parameters $\sin^2\theta_{23}$ and Δm^2_{31} obtained from the three-neutrino analysis of atmospheric neutrino data (after minimizing over θ_{13}) are given by the black lines in Fig. 2. The preferred values for the oscillation parameters for normal (inverted) mass ordering given by the atmospheric data only are located at:

$$\sin^2\theta_{23} = 0.50\,(0.53)\,, \quad \Delta m^2_{31} = 2.11\times10^{-3}\ \text{eV}^2\,(2.11\times10^{-3}\ \text{eV}^2)\,. \tag{3}$$

3.2 Long-baseline neutrino experiments

Several long-baseline accelerator neutrino experiments have been proposed to probe the ν_μ disappearance oscillation channel in the same region of Δm^2 as explored by atmospheric neutrinos. In this section we

will discuss the results of the KEK to Kamioka (K2K) and the Main Injector Neutrino Oscillation Search (MINOS) experiments.

In K2K the neutrino beam is produced by a 12 GeV proton beam from the KEK proton synchrotron, and consists of 98% muon neutrinos with a mean energy of 1.3 GeV. The beam is controlled by a near detector 300 m away from the proton target. Information on neutrino oscillations is obtained by the comparison of the near detector data with the ν_μ content of the beam observed by the Super-Kamiokande detector at a distance of 250 km. In our global analysis we include the two data samples released by the K2K Collaboration, K2K-I and K2K-II, collected in the period from June 1999 to July 2001 and from December 2002 to November 2004, respectively [23]. From the combined analysis of K2K-I and K2K-II, 112 events have been observed in Super-Kamiokande, whereas $158.1^{+9.2}_{-8.6}$ were expected for no oscillations. This gives a clear proof for ν_μ disappearance (the probability that the observations are explained by a statistical fluctuation without neutrino oscillations is 0.0015%). Moreover, the spectral distortion expected for oscillations has been seen through the energy reconstruction of the 58 single-ring muon events observed. More details about our treatment of the K2K data can be found in Ref. [24].

MINOS is a long-baseline experiment that searches for ν_μ disappearance in a neutrino beam with a mean energy of 3 GeV produced at Fermilab. It consists of a near detector, located at 1 km from the neutrino source and a far detector located at the Soudan Mine, at 735 km from Fermilab. Here we consider the results for ν_μ disappearance from the MINOS experiment with an accumulated exposure of 7.25×10^{20} protons-on-target (p.o.t.) [25]. The energy neutrino spectra relevant for the analysis of neutrino oscillations is presented in 27 energy bins between 0 and 10 GeV. In our re-analysis of MINOS data we fit the event spectrum within a full three-flavour framework using the GLoBES software [26] to simulate the experiment. Backgrounds provided by the MINOS collaboration are included in our simulation, together with a total systematic uncertainty of 5% and an energy resolution of 15%, in order to reproduce the two-flavour allowed regions obtained by MINOS. In addition to matter effects, we include also the effect of Δm^2_{21} as well as θ_{13} and the CP-phase δ in the analysis of the disappearance and appearance channels [1]. The tension between the muon neutrino and muon antineutrino measurements reported by the MINOS Collaboration in [27] has now been clarified after the improved measurement of muon antineutrino disappearance published in [28], which showed that both data samples are compatible. However, since the statistics of muon antineutrino disappearance is still rather weak compared with the oscillations in the neutrino channel we only include this later channel in our global fit.

The allowed regions for the combined analysis of K2K and MINOS data are shown in Fig. 2 in comparison to the ones from atmospheric neutrino data only. This figure illustrates that the neutrino mass-squared difference indicated by the ν_μ disappearance observed in long-baseline experiments is in perfect agreement with atmospheric neutrino oscillations. Hence, K2K and MINOS provide a confirmation of oscillations with Δm^2_{31} from an artificial neutrino source. Note here that current MINOS data largely surpass the pioneering K2K observations which by now give only a very minor contribution to the neutrino parameter determinations.

3.3 Combined atmospheric + long-baseline analysis

Combining the atmospheric and long-baseline neutrino data from K2K and MINOS we obtain improved constraints on the atmospheric neutrino oscillation parameters. The results from the combined analysis are shown in the red/shadowed regions of Fig. 2. There we can see that currently the determination of the atmospheric parameters is mostly dominated by long-baseline data (mainly MINOS). However, the information coming from atmospheric data is still very important to constrain the mixing angle θ_{23}, as well as θ_{13}. We find the following best fit values with errors at 1σ for normal (NH) and inverted (IH) mass

[1] The searches for electron neutrino appearance at the long-baseline accelerator experiments MINOS and T2K will be presented in Sect. 4, when discussing the determination of the reactor mixing angle θ_{13}

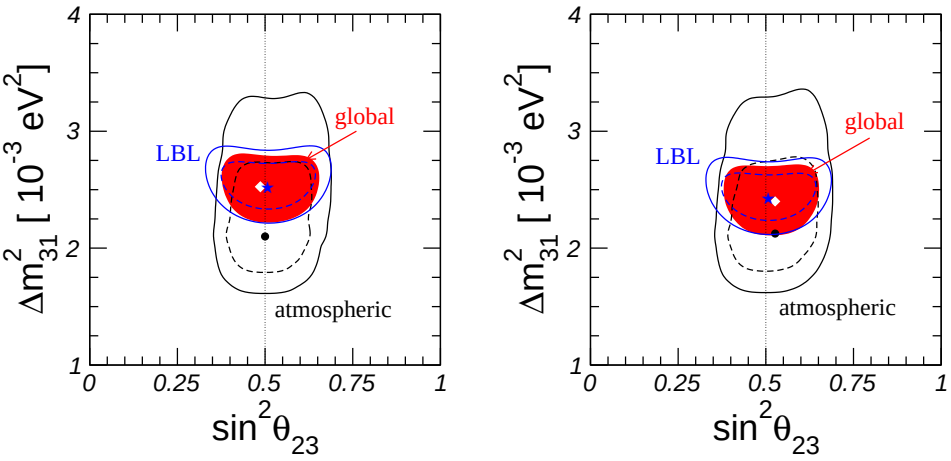

Fig. 2 Determination of the atmospheric oscillation parameters by the interplay of atmospheric (black) and LBL disappearance (blue) data at 90% CL (dashed) and 3σ (solid) for 2 dof. The 3σ constraints resulting from the combined analysis are shown in the red/shaded region. The left panel corresponds to the normal hierarchy while the left one shows the results for the inverted mass ordering.

hierarchy:

$$\sin^2\theta_{23} = \begin{cases} 0.49^{+0.08}_{-0.05} & \text{(NH)} \\ 0.53^{+0.05}_{-0.07} & \text{(IH)} \end{cases} \tag{4}$$

$$|\Delta m^2_{31}| = \begin{cases} 2.53^{+0.08}_{-0.10} \times 10^{-3}\,\text{eV}^2 & \text{(NH)} \\ 2.49^{+0.10}_{-0.07} \times 10^{-3}\,\text{eV}^2 & \text{(IH)} \end{cases} \tag{5}$$

Notice that, due to the definition of the neutrino mass splittings in a three-neutrino scheme, the sub-leading effects of Δm^2_{21} lead to different best fit points for $|\Delta m^2_{31}|$, depending on the neutrino mass hierarchy. The reason for this apparent shift in $|\Delta m^2_{31}|$ is a result of our parameterization since for NH the largest frequency is given by $|\Delta m^2_{31}|$, while in IH it is $|\Delta m^2_{31}| + \Delta m^2_{21}$, which explains why $|\Delta m^2_{31}|$ is smaller for IH. The present 1σ uncertainties on Δm^2_{31} given in Eq. (5) are at the level of this sub-leading effect and therefore it should be included in our analysis of long-baseline data.

4 The reactor angle θ_{13}

For a long period the reactor mixing angle θ_{13} has been the only unknown neutrino oscillation parameter. Unlike for the rest of parameters, θ_{13} was not measured since no neutrino oscillations driven by this parameter were observed. In fact, until last year the most accurate information about the reactor mixing angle was an upper-bound coming from the non-observation of reactor antineutrino disappearance at the CHOOZ reactor experiment [29]:

$$\sin^2\theta_{13} < 0.039 \tag{6}$$

at 90% CL for $\Delta m^2_{31} = 2.5 \times 10^{-3}\text{eV}^2$.

Nevertheless, the precise determination of this parameter is crucial for the development of the future neutrino oscillation experiments, since it controls the size of the matter effects and the CP-violating factor in the oscillation probabilities relevant for the atmospheric and long-baseline experiments. In consequence, a large effort has been concentrated in the determination of this angle either through the searches for electron neutrino appearance at accelerator experiments as well as through the design of a new generation of reactor experiments.

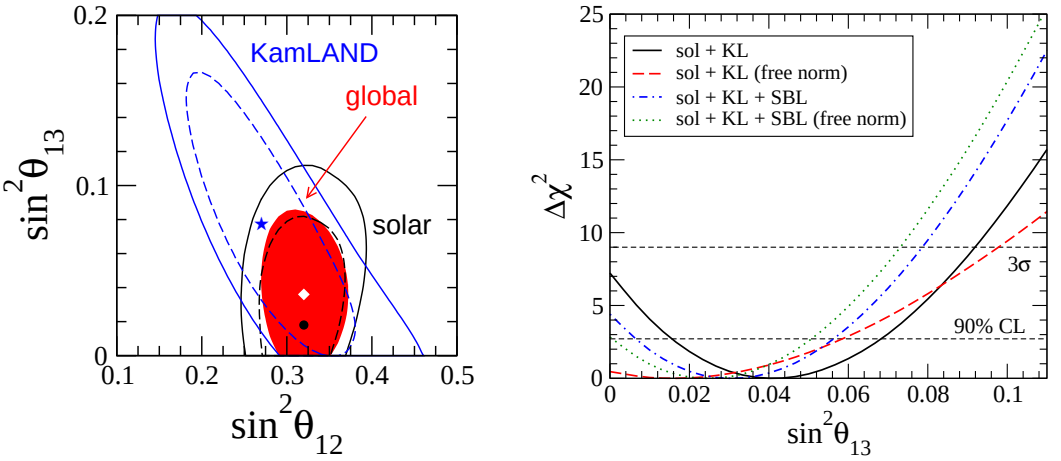

Fig. 3 Left: Allowed regions in the (θ_{12} - θ_{13}) plane at 90% and 99% CL (2 dof) for solar and KamLAND, as well as the 99% CL region for the combined analysis. Δm^2_{21} has been minimized out. The dot, star and diamond indicate the best fit points for solar, KamLAND and combined data, respectively. Right: $\Delta\chi^2$ as a function of $\sin^2\theta_{13}$ for the solar + KamLAND analysis using different assumptions on the reactor data analysis.

4.1 Hints on non-zero θ_{13} from global analysis

The interplay between different data samples in a global neutrino oscillation fit has shown some sensitivity to the reactor mixing angle θ_{13}. In particular, from the combined analysis of solar and KamLAND neutrino data, a non-zero θ_{13} value is preferred:

$$\sin^2\theta_{13} = 0.035^{+0.016}_{-0.015} \quad \text{(solar + KamLAND)} \tag{7}$$

with $\Delta\chi^2(\sin^2\theta_{13} = 0)$ = 5.4, and therefore a 2.3σ hint for $\theta_{13} \neq 0$ coming from the solar sector. This non-trivial constraint on θ_{13} comes mainly from the preference of KamLAND data for a non-zero θ_{13} (visible in the left panel of Fig. 3), but also from the different correlation between $\sin^2\theta_{13}$ and $\sin^2\theta_{12}$ present in the solar and KamLAND neutrino data samples [24, 30]. On the other hand, a non-zero value of θ_{13} helps to reconcile the slightly different best fit points for Δm^2_{21} for solar and KamLAND separately.

In the left panel of Fig. 3 we show the 90% and 99% CL allowed regions in the $\sin^2\theta_{12} - \sin^2\theta_{13}$ plane from the analysis of solar and KamLAND data as well as from the combined solar + KamLAND analysis. This result depends on the assumptions made on the reactor data analysis, as shown in the right panel of Fig. 3, where different constraints on θ_{13} from the combination of solar and KamLAND are obtained. In particular, the best fit value for $\sin^2\theta_{13}$ may range from 0.035 (for the "sol + KL" case in the left panel and black/solid line in the right panel) to 0.023 (for the "sol + KL + SBL (free norm)" case in the green/dotted line of right panel), see Ref. [3] for a detailed discussion. However, the impact of these differences over the global neutrino analysis is very mild since the global determination of θ_{13} is dominated by the recent measurements at the new reactor experiments, as we will see.

An additional hint for a non-zero value of θ_{13} can be obtained from the combination of atmospheric and long-baseline neutrino data [31, 32]. Atmospheric neutrino data from Super-Kamiokande I+II+III described in the previous section implies a best fit point very close to $\theta_{13} = 0$ [22], with $\Delta\chi^2 = 0.0(0.3)$ for $\theta_{13} = 0$ for NH (IH). However, in the combination with the accelerator neutrino data from MINOS we find a slight preference for $\theta_{13} > 0$, with $\Delta\chi^2 = 1.6(1.9)$ at $\theta_{13} = 0$ for NH (IH) [3]. As shown in Fig. 4 this happens due to a small mismatch of the best fit values for $|\Delta m^2_{31}|$ at $\theta_{13} = 0$, which can be resolved by allowing for non-zero values of θ_{13} [33].

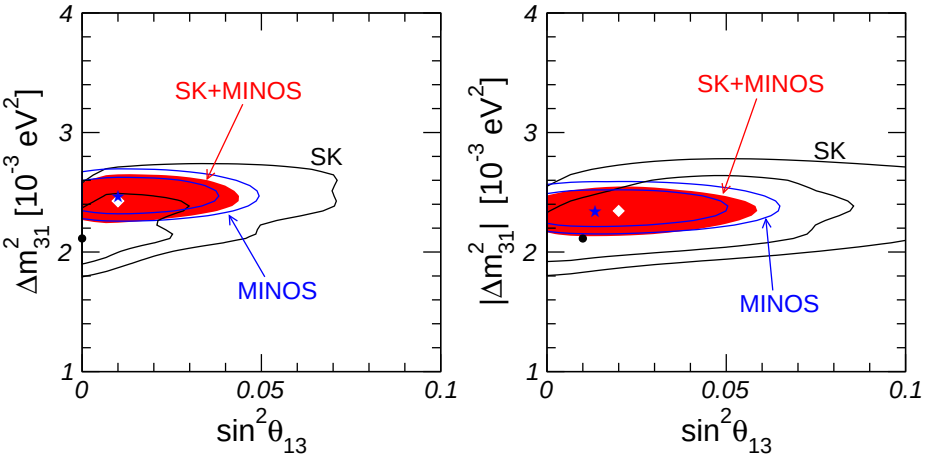

Fig. 4 Allowed regions at 1σ and 90% CL for atmospheric (SK) and MINOS data in the plane of $\sin^2\theta_{13}$ and Δm^2_{31} for NH (left) and IH (right). Combined data is shown as shaded/red region at 90% CL. The black dot, blue star, white diamond correspond to the best fit points of SK, MINOS, SK+MINOS, respectively.

4.2 Searches for ν_e appearance at long-baseline experiments

In our global analysis of neutrino oscillation data we include the latest ν_e appearance data from the long-baseline accelerator experiments MINOS and T2K. At leading order, the $\nu_\mu \to \nu_e$ oscillation probability at long-baseline experiments is given by the following expression:

$$P_{\nu e} = \sin^2 2\theta_{13} \sin^2\theta_{23} \sin^2\left(\frac{\Delta m^2_{31} L}{4E}\right) + ... \tag{8}$$

Therefore, the observation of ν_e appearance in an almost pure ν_μ beam provides a clear evidence for a non-zero θ_{13}. Sub-leading terms not explicitly shown in Eq. (8) depend on the CP-violating phase δ and then, some sensitivity to this parameter will also be obtained from the analysis of appearance neutrino data.

The MINOS Collaboration has reported data from the search of $\nu_\mu \to \nu_e$ transitions in the Fermilab NuMI beam [34] corresponding to 8.2×10^{20} protons on target. MINOS finds 62 events with an expectation in absence of oscillations of 49.6 ± 7.0(stat) $\pm$ 2.7(syst), showing a 1.7σ excess of electron neutrinos over the expected background. We fit the MINOS ν_e spectrum by using the GLoBES simulation software [26], where we calibrate our predicted spectrum by using the information given in [35]. A full three-flavour fit is performed taking into account a 5% uncertainty on the matter density along the neutrino path.

The Tokai to Kamioka (T2K) experiment uses a neutrino beam consisting mainly of muon neutrinos, produced at the J-PARC accelerator facility and observed at a distance of 295 km and an off-axis angle of 2.5° by the Super-Kamiokande detector. The present data release corresponds to 1.43×10^{20} protons on target [36]. Six events pass all selection criteria for an electron neutrino event. In a three-flavor neutrino oscillation scenario with $\theta_{13} = 0$ the expected number of such events is 1.5 ± 0.3 (syst). Under this hypothesis, the probability to observe six or more candidate events is 7×10^{-3}, equivalent to a significance of 2.5σ. Analogously to the case of MINOS, our simulation of T2K neutrino spectrum is performed with GLoBES. We use the neutrino fluxes predicted at Super-Kamiokande in the absence of oscillations to calculate the $\nu_\mu \to \nu_e$ appearance signal, tuning our simulation to the corresponding prediction given in Ref. [36]. In the fit we include the background distribution as well as a systematic normalization uncertainty of 23% and a 5% uncertainty on the matter density and we adopt the χ^2 definition based on the Poisson distribution.

In Fig. 5 we show the region in the $\sin^2\theta_{13} - \delta$ plane indicated by MINOS data in comparison to T2K results. For T2K we obtain a closed region for $\sin^2\theta_{13}$ at 90% CL ($\Delta\chi^2 = 2.7$), while for MINOS we find only an upper bound on $\sin^2\theta_{13}$. The results are clearly compatible and we show the combined analysis

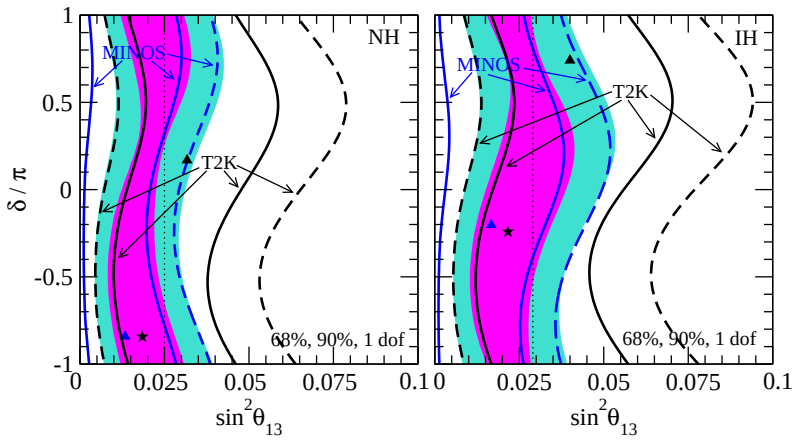

Fig. 5 Regions in the $\sin^2\theta_{13} - \delta$ plane at 68% and 90% CL (1 dof) for T2K and MINOS appearance data (curves) and their combination (shaded regions). For all other oscillation parameters we assume best fit values and uncertainties according to Tab. 1. The left (right) panel is for normal (inverted) mass hierarchy.

as shaded regions, where the upper bound is determined by the MINOS constraint while the lower bound is given by T2K. Best fit values are in the range $\sin^2\theta_{13} \approx 0.015 - 0.023$, depending on the CP phase δ, where the variation is somewhat larger for the inverted mass hierarchy.

4.3 New generation of reactor experiments

Compared to their predecessors, the new reactor experiments have larger statistics, thanks to their increased reactor power and the bigger antineutrino detector size. On the other hand, one of their most important features is that they have identical antineutrino detectors located at different distances from the reactor core. As a result measurements at the closest detectors can be used to predict the expected event number at the more distant detectors, avoiding to rely on theoretical calculations of the produced antineutrino flux at the reactors. Currently, three reactor experiments of this kind are running in Europe and Asia: Double Chooz, Daya Bay and RENO. Along this year the three experiments have for the first time observed the disappearance of reactor antineutrinos over short distances, providing the first measurement of the mixing angle θ_{13}, so far unknown.

The Double Chooz (DC) experiment, in France, is a reactor experiment planned to have two detectors and two reactors. In its first stage DC has reported 101 days of running [37], with only the far detector operating so far. The near detector (ND) is expected to start operation by the end of 2013. The two reactor have an individual power of 4.25 GW_{th} and are placed at a distance of 1050 m from the far detector. The detector has a fiducial volume of 10 m^3 of neutrino target liquid. From the analysis of the rate and the energy spectrum of the prompt positrons produced by the reactor antineutrinos, the DC collaboration find $\sin^2 2\theta_{13} = 0.086 \pm 0.041(\text{stat}) \pm 0.030(\text{syst})$. Using only the ratio of observed to expected events a slightly higher best fit value is obtained: $\sin^2 2\theta_{13} = 0.104 \pm 0.030(\text{stat}) \pm 0.076(\text{syst})$

The Daya Bay (DYB) reactor experiment [38] is placed in China and it contains an array of three groups of detectors and three groups of two-reactor cores. The far group of detectors (far hall) is composed of three detectors and the two near halls are composed by one and two detectors, respectively. The antineutrino detectors are approximately equal, with a volume of 20 ton of Gadolinium-doped liquid scintillator as neutrino target material. The six reactor cores are approximately equal as well, with a maximum individual power of 2.9 GW_{th}. The distances to the detectors range from 350 to 2000 m approximately. The rate-only analysis performed by the DYB collaboration finds a best fit value of $\sin^2 2\theta_{13} = 0.092 \pm 0.016(\text{stat}) \pm 0.005(\text{syst})$. A zero value for θ_{13} is excluded with a significance of 5.2σ

The RENO experiment [39] is situated in South Korea and it has been running for 229 days. It consists of six reactor cores, distributed along a 1.3 km straight line. Two of the reactors have a maximum power of

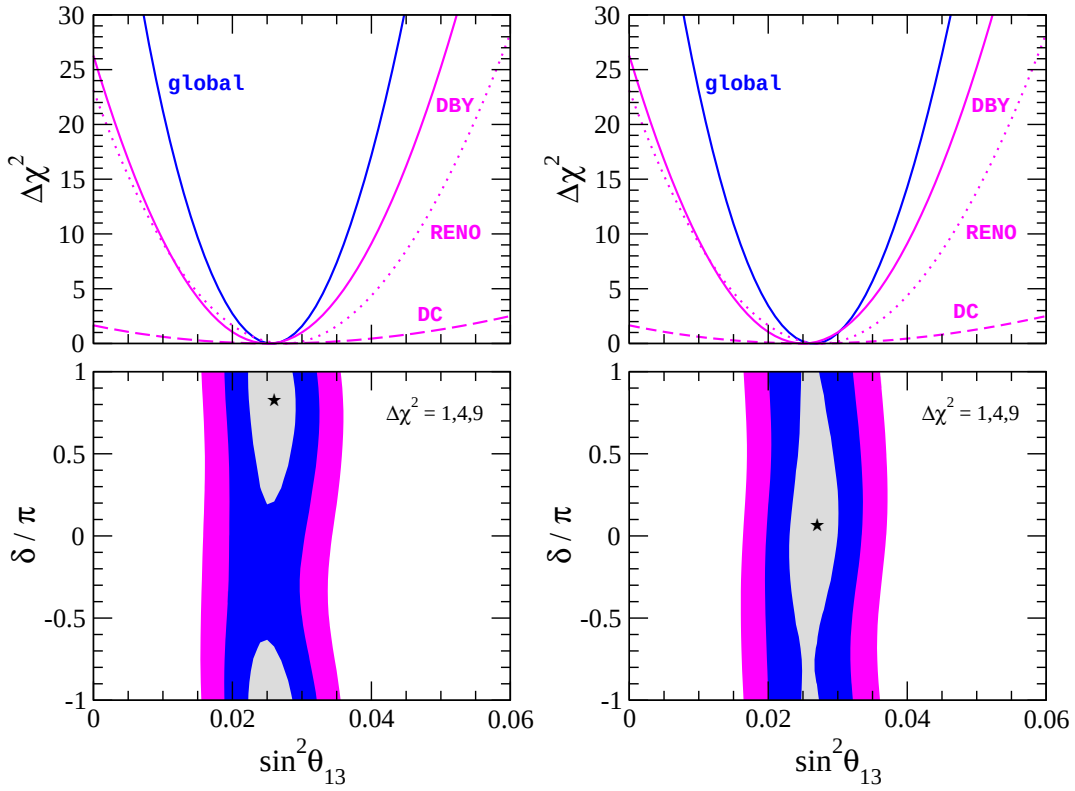

Fig. 6 Upper panels: $\Delta\chi^2$ as a function of $\sin^2\theta_{13}$ from the analysis of the total event rate in Daya Bay (solid magenta/light line), RENO (dotted line) and Double Chooz (dashed line) as well as from the analysis of global neutrino data (solid blue/dark line). Lower panels: contours of $\Delta\chi^2 = 1, 4, 9$ in the $\sin^2\theta_{13} - \delta$ plane from the global fit to the data. We minimize over all undisplayed oscillation parameters. Left (right) panels are for normal (inverted) neutrino mass hierarchy.

2.66 $\mathrm{GW_{th}}$ while the other four may reach 2.8 $\mathrm{GW_{th}}$. Reactor antineutrinos are detected by two identical detectors, located at 294 and 1383 m from the reactor array center. Each RENO detector contains 16 ton of Gadolinium-doped Liquid Scintillator. Based on a rate-only analysis, the RENO Collaboration finds $\sin^2 2\theta_{13} = 0.113 \pm 0.013(\mathrm{stat.}) \pm 0.019(\mathrm{syst.})$, together with a 4.9σ exclusion for $\theta_{13} = 0$.

In order to minimize the dependence upon the predicted normalization of the antineutrino spectrum, we analyze the total rate of expected events at the far detector/s in the presence of oscillations over the no–oscillation prediction. This way, our statistical analysis is free of correlations among the different reactor data samples, since the relative measurements do not rely on flux predictions. Details about the reactor event simulation and the analysis of reactor data can be found at Ref. [1]. The $\Delta\chi^2$ profiles as a function of θ_{13} obtained for each reactor experiment are shown in the upper panels pf Fig. 6. As expected, the more constraining results are coming from the Daya Bay and RENO experiments, while Double Chooz has still a reduced sensitivity to θ_{13}.

5 Results from the three-neutrino global analysis

Here we summarize the results for the neutrino oscillation parameters obtained in the global analysis to neutrino data in Ref. [1]. Details on the numerical analysis of all the neutrino samples can be found there and in our previous works in Refs. [2, 3, 14, 24].

The results obtained for $\sin^2\theta_{13}$ and δ are summarized in Fig. 6. In the upper panels we show the $\Delta\chi^2$ profile as a function of $\sin^2\theta_{13}$ for normal (left panel) and inverted (right panel) neutrino mass hierarchies. The solid blue/dark line corresponds to the result obtained from the combination of all the data samples while the others correspond to the individual reactor data samples, as indicated. One sees from the constraints on $\sin^2\theta_{13}$ coming from each of the new reactor experiments separately [2] that the global constraint on θ_{13} is dominated by the recent Daya Bay and RENO measurements. For both neutrino mass hierarchies we find that the 3σ indication for $\theta_{13} > 0$ obtained in our previous work [2] due mainly to the first indications observed by MINOS and T2K is now overwhelmingly confirmed as a result of the recent reactor data. Thus, in our global fit we obtain a $\Delta\chi^2 = 64.3(65.0)$, resulting in a 8.02σ (8.06σ) exclusion of $\theta_{13} = 0$ for normal (inverted) mass hierarchy.

In the lower panels of Fig. 6 we show the contours of $\Delta\chi^2 = 1, 4, 9$ in the $\sin^2\theta_{13} - \delta$ plane from the global fit to the neutrino oscillation data. In this plane we find the following best fit points:

$$\begin{array}{lll} \sin^2\theta_{13} = 0.026\,, & \delta = 0.83\pi & \text{(normal hierarchy)}, \\ \sin^2\theta_{13} = 0.027\,, & \delta = 0.07\pi & \text{(inverted hierarchy)}. \end{array} \tag{9}$$

One can also see that, in the normal mass hierarchy case, at $\Delta\chi^2 = 1$ a "preferred region" for the CP phase δ emerges from the complementarity between MINOS and T2K appearance data. For the case of inverse hierarchy no preferred region appears at the χ^2 cuts shown in the figure. Obviously this preference for the CP phase in NH is not yet significant. Marginalizing over δ (and all other oscillation parameters), obtaining for the best fit, one-sigma errors, and the significance for $\theta_{13} > 0$:

$$\begin{array}{lll} \sin^2\theta_{13} = 0.026^{+0.003}_{-0.004}\,, & \Delta\chi^2 = 64.3\,(8.02\sigma) & \text{(normal)}, \\ \sin^2\theta_{13} = 0.027^{+0.003}_{-0.004}\,, & \Delta\chi^2 = 65.0\,(8.06\sigma) & \text{(inverted)}. \end{array} \tag{10}$$

Besides θ_{13} and δ, from the global analysis of neutrino data we also calculate the best fit values and ranges allowed for all the other neutrino oscillation parameters. Our results are summarized in Fig. 7 and Table 1. Comparing with previous results we see that the inclusion of the new reactor data does

parameter	best fit $\pm 1\sigma$	2σ	3σ
Δm^2_{21} $[10^{-5}\text{eV}^2]$	7.62 ± 0.19	7.27–8.01	7.12–8.20
Δm^2_{31} $[10^{-3}\text{eV}^2]$	$2.53^{+0.08}_{-0.10}$ $-(2.40^{+0.10}_{-0.07})$	$2.34 - 2.69$ $-(2.25 - 2.59)$	$2.26 - 2.77$ $-(2.15 - 2.68)$
$\sin^2\theta_{12}$	$0.320^{+0.015}_{-0.017}$	0.29–0.35	0.27–0.37
$\sin^2\theta_{23}$	$0.49^{+0.08}_{-0.05}$ $0.53^{+0.05}_{-0.07}$	0.41–0.62 0.42–0.62	0.39–0.64
$\sin^2\theta_{13}$	$0.026^{+0.003}_{-0.004}$ $0.027^{+0.003}_{-0.004}$	0.019–0.033 0.020–0.034	0.015–0.036 0.016–0.037
δ	$\left(0.83^{+0.54}_{-0.64}\right)\pi$ 0.07π [3]	$0 - 2\pi$	$0 - 2\pi$

Table 1 Neutrino oscillation parameters summary. For Δm^2_{31}, $\sin^2\theta_{23}$, $\sin^2\theta_{13}$, and δ the upper (lower) row corresponds to normal (inverted) neutrino mass hierarchy. [3]Note that in this case the full (0,2π) range is allowed.

not have a strong impact on the determination of all the remaining neutrino oscillation parameters, which were already pretty well determined by solar, atmospheric, long–baseline and KamLAND reactor data. As stated above, the sensitivity of current neutrino data to the CP phase δ is still very poor and therefore

[2] Here we have fixed all the other oscillation parameters to their best fit values.

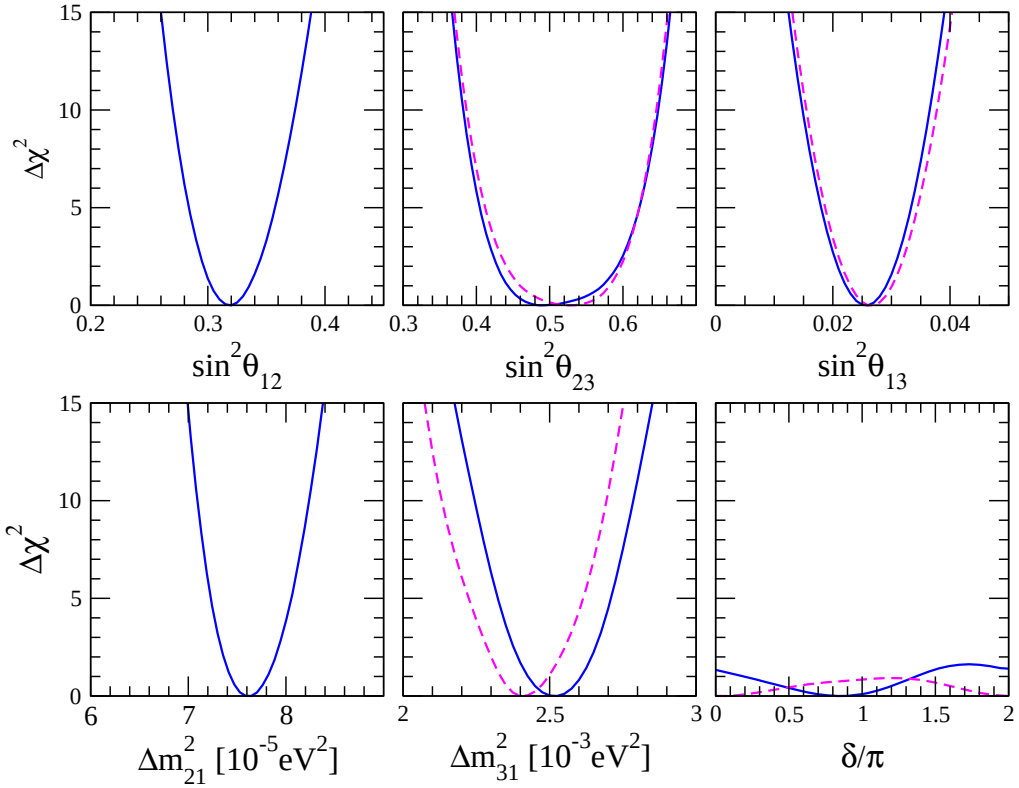

Fig. 7 $\Delta\chi^2$ profiles as a function of all the neutrino oscillation parameters $\sin^2\theta_{12}$, $\sin^2\theta_{23}$, $\sin^2\theta_{13}$, Δm^2_{21}, Δm^2_{31} and δ. For the central and right panels the solid lines correspond to the case of normal mass hierarchy while the dashed lines correspond to the results for the inverted mass hierarchy.

nothing can be said about its value. The same affirmation holds for the neutrino mass hierarchy, since present neutrino data do not show a preference for any of the two possible mass orderings. We find that inverted hierarchy gives a slightly better fit, however, with only $\Delta\chi^2 \sim 1.4$ with respect to the best fit in normal hierarchy. Concerning the atmospheric neutrino mixing angle, global neutrino data so far do not show a definite preference for a given octant of θ_{23}. Our results in Table 1 show a slight preference for the first octant in the case of normal hierarchy, while the second octant is somewhat preferred for inverse hierarchy. Note however that the indication for the first or second octant is still rather marginal for both hierarchies and no significant preference can be extracted from the data [4].

6 Summary and future prospects

In this work we have summarized the current status of the three-neutrino oscillation parameters, including the most recent data from all solar, atmospheric, accelerator and reactor neutrino experiments. The most remarkable result reported in this analysis is the first measurement of the reactor mixing angle θ_{13} made by the new generation of reactor experiments. From the global fit to neutrino data we have found a best fit value of $\sin^2\theta_{13} = 0.026(0.027)$ for normal (inverted) neutrino mass hierarchy, while $\sin^2\theta_{13} = 0$ is now excluded at 8σ. The impact of the new θ_{13} measurements over the other neutrino oscillation parameters is marginal since they are already quite well determined by solar, atmospheric, long–baseline and KamLAND

[4] This would presumably change after the update of our global analysis with the new MINOS data presented in the Neutrino 2012 Conference, since they show a preference for non-maximal neutrino mixing.

reactor data. No significant sensitivity to the CP-violating phase δ or the neutrino mass ordering has been found by the combination of all current neutrino data. The results are summarized in Table 1.

After the accurate measurements of the neutrino oscillation parameters presented in last section, it is obvious that the time for precision measurements has arrived. In particular, a precise determination of θ_{13} will be a crucial ingredient towards a new era of CP violation searches in neutrino oscillations [41,42] and will also help determining the neutrino mass hierarchy.

Starting with the reactor mixing angle θ_{13}, an improved measurement is expected very soon from the statistically updated data sample in Double Chooz, Daya Bay and RENO reactor experiments. Further improvement will be obtained after the completion of the Daya Bay designed number of detectors by adding one detector in the far hall and other one in one of the near halls this summer. After 3 years of operation the Daya Bay uncertainties on $\sin^2 2\theta_{13}$ will be reduced from 20% to 4-5% [40]. The installation of the near detector in Double Chooz expected by the end of 2013 will also help understanding the spectral distortions in the reactor neutrino spectrum.

Muon-neutrino disappearance results from the T2K and NOνA long-baseline accelerator experiments will improve the determination of the atmospheric mass splitting $|\Delta m^2_{31}|$ at the level of a few percent [43–45]. The atmospheric mixing angle θ_{23} is also likely to be measured with improved precision. Regarding the deviations of θ_{23} from maximal mixing, a combination of future accelerator and reactor neutrino data may help to solve the ambiguity between the first and second octant [46].

Several ideas have been proposed to address the issue of the neutrino mass ordering. One of them [47] exploits the sensitivity to matter effects of the accelerator experiment NOνA and the atmospheric neutrino observations at the future India-based Neutrino Observatory (INO) experiment [48]. A combined analysis of the two experiments would allow a 2σ rejection of the wrong mass hierarchy by 2020 [47]. The possibility of identifying the neutrino mass hierarchy with a reactor neutrino experiment at an intermediate baseline ($\sim$ 60 km) has ben discussed in Refs. [49, 50].

Note added: After the completion of this work, new neutrino oscillation data have been presented at the Neutrino 2012 Conference in Kyoto (Japan). An updated global analysis including the relevant neutrino data will be published in [1].

Acknowledgements I would like to thank my collaborators T. Schwetz, J. W. F. Valle and D. V. Forero with whom part of this work has been done. This work was supported by CSIC under the JAE-Doc programme (co-funded by the European Social Fund), the Spanish MEC under grants FPA2011-22975 and MULTIDARK CSD2009-00064 (Consolider-Ingenio 2010 Programme) and Prometeo/2009/091 (Generalitat Valenciana).

References

[1] D. V. Forero, M. Tortola and J. W. F. Valle, arXiv:1205.4018 [hep-ph].
[2] T. Schwetz, M. Tortola and J. W. F. Valle, New J. Phys. **13**, 109401 (2011) [arXiv:1108.1376 [hep-ph]].
[3] T. Schwetz, M. Tortola and J. W. F. Valle, New J. Phys. **13**, 063004 (2011) [arXiv:1103.0734 [hep-ph]].
[4] B. T. Cleveland *et al.*, Astrophys. J. **496**, 505 (1998).
[5] F. Kaether *et al.*, Phys. Lett. B **685**, 47 (2010) [arXiv:1001.2731 [hep-ex]].
[6] SAGE Collaboration, J. N. Abdurashitov *et al.*, Phys. Rev. C **80**, 015807 (2009) [arXiv:0901.2200 [nucl-ex]].
[7] Super-Kamiokande Collaboration, J. Hosaka *et al.*, Phys. Rev. D **73**, 112001 (2006), [hep-ex/0508053].
[8] Super-Kamiokande Collaboration, J. P. Cravens *et al.*, Phys. Rev. D **78**, 032002 (2008) [arXiv:0803.4312].
[9] Super-Kamiokande Collaboration, K. Abe *et al.*, Phys. Rev. D **83**, 052010 (2011) [arXiv:1010.0118 [hep-ex]].
[10] SNO Collaboration, B. Aharmim *et al.*, Phys. Rev. Lett. **101**, 111301 (2008) [arXiv:0806.0989 [nucl-ex]].
[11] SNO Collaboration, B. Aharmim *et al.*, Phys. Rev. C **81**, 055504 (2010) [arXiv:0910.2984 [nucl-ex]].
[12] Borexino Collaboration, C. Arpesella *et al.*, Phys. Rev. Lett. **101**, 091302 (2008) [arXiv:0805.3843 [astro-ph]].
[13] A. Serenelli, S. Basu, J. W. Ferguson and M. Asplund, Astrophys. J. **705**, L123 (2009) [arXiv:0909.2668].
[14] T. Schwetz, M. A. Tortola and J. W. F. Valle, New J. Phys. **10** (2008) 113011 [arXiv:0808.2016v3 [hep-ph]].
[15] M. Maltoni, T. Schwetz, M. A. Tortola and J. W. F. Valle, Phys. Rev. **D68**, 113010 (2003), [hep-ph/0309130].
[16] G. L. Fogli *et al.*, Phys. Rev. D **66**, 053010 (2002), [hep-ph/0206162].

[17] KamLAND Collaboration, K. Eguchi *et al.,* Phys. Rev. Lett. **90**, 021802 (2003), [hep-ex/0212021].
[18] KamLAND Collaboration, A. Gando *et al.*, Phys. Rev. D **83**, 052002 (2011) [arXiv:1009.4771 [hep-ex]].
[19] T. A. Mueller *et al.*, Phys. Rev. C **83**, 054615 (2011) [arXiv:1101.2663 [hep-ex]].
[20] Super-Kamiokande Collaboration, Y. Fukuda *et al.*, Phys. Rev. Lett. **81**, 1562 (1998) [hep-ex/9807003].
[21] Super-Kamiokande Collaboration, Y. Ashie *et al.*, Phys. Rev. Lett. **93**, 101801 (2004) [hep-ex/0404034].
[22] Super-Kamiokande Collaboration, R. Wendell *et al.*, Phys. Rev. D **81**, 092004 (2010) [arXiv:1002.3471].
[23] K2K Collaboration, M. H. Ahn *et al.*, Phys. Rev. D **74**, 072003 (2006) [hep-ex/0606032].
[24] M. Maltoni, T. Schwetz, M. A. Tortola and J. W. F. Valle, New J. Phys. **6**, 122 (2004) [hep-ph/0405172].
[25] MINOS Collaboration, P. Adamson *et al.*, Phys. Rev. Lett. **106**, 181801 (2011) [arXiv:1103.0340 [hep-ex]].
[26] P. Huber *et al.*, Comput. Phys. Commun. **177** (2007) 432 [arXiv:hep-ph/0701187].
[27] MINOS Collaboration, P. Adamson *et al.*, Phys. Rev. Lett. **107**, 021801 (2011) [arXiv:1104.0344 [hep-ex]].
[28] MINOS Collaboration, P. Adamson *et al.*, Phys. Rev. Lett. **108**, 191801 (2012) [arXiv:1202.2772 [hep-ex]].
[29] CHOOZ Collaboration, M. Apollonio *et al.,* Eur. Phys. J. **C27**, 331 (2003), [hep-ex/0301017].
[30] S. Goswami and A. Y. Smirnov, Phys. Rev. D **72**, 053011 (2005) [hep-ph/0411359].
[31] G. L. Fogli, E. Lisi, A. Marrone and A. Palazzo, Prog. Part. Nucl. Phys. **57**, 742 (2006) [hep-ph/0506083].
[32] J. Escamilla, D. C. Latimer and D. J. Ernst, Phys. Rev. Lett. **103**, 061804 (2009) [arXiv:0805.2924 [nucl-th]].
[33] M. C. Gonzalez-Garcia, M. Maltoni and J. Salvado, JHEP **1004**, 056 (2010) [arXiv:1001.4524 [hep-ph]].
[34] MINOS Collaboration, P. Adamson *et al.*, Phys. Rev. Lett. **107**, 181802 (2011) [arXiv:1108.0015 [hep-ex]].
[35] J. A. A. Boehm. Measurement of electron neutrino appearance with the MINOS experiment. FERMILAB-THESIS-2009-17.
[36] T2K Collaboration, K. Abe *et al.*, Phys. Rev. Lett. **107**, 041801 (2011) [arXiv:1106.2822 [hep-ex]].
[37] Double Chooz Collaboration, Y. Abe *et al.*, Phys. Rev. Lett. **108**, 131801 (2012) [arXiv:1112.6353 [hep-ex]].
[38] Daya Bay Collaboration, F. P. An *et al.*, Phys. Rev. Lett. **108**, 171803 (2012) [arXiv:1203.1669 [hep-ex]].
[39] RENO Collaboration, J. K. Ahn *et al.*, Phys. Rev. Lett. **108**, 191802 (2012) [arXiv:1204.0626 [hep-ex]].
[40] J. Cao's talk at nuTURN2012 - Neutrino at the Turning Point, Gran Sasso, May 2012.
[41] H. Nunokawa, S. J. Parke and J. W. F. Valle, Prog. Part. Nucl. Phys. **60**, 338 (2008) [arXiv:0710.0554 [hep-ph]].
[42] ISS Physics Working Group, A. Bandyopadhyay *et al.*, Rept. Prog. Phys. **72**, 106201 (2009) [arXiv:0710.4947].
[43] K. Abe *et al.* [T2K Collaboration], Nucl. Instrum. Meth. A **659**, 106 (2011) [arXiv:1106.1238 [physics.ins-det]].
[44] D. S. Ayres *et al.* [NOvA Collaboration], hep-ex/0503053.
[45] P. Huber, M. Lindner, M. Rolinec, T. Schwetz and W. Winter, Phys. Rev. D **70**, 073014 (2004) [hep-ph/0403068].
[46] P. Huber, M. Lindner, T. Schwetz and W. Winter, JHEP **0911**, 044 (2009) [arXiv:0907.1896 [hep-ph]].
[47] M. Blennow and T. Schwetz, arXiv:1203.3388 [hep-ph].
[48] http://www.imsc.res.in/ ino/
[49] S. T. Petcov and M. Piai, Phys. Lett. B **533**, 94 (2002) [hep-ph/0112074].
[50] L. Zhan, Y. Wang, J. Cao and L. Wen, Phys. Rev. D **78**, 111103 (2008) [arXiv:0807.3203 [hep-ex]].